Medical & Biological Engineering & Computing (2018) 56:1823–1839
https://doi.org/10.1007/s11517-018-1813-4

ORIGINAL ARTICLE

A generalised porous medium approach to study thermo-fluid dynamics in human eyes

Alessandro Mauro[1] · Nicola Massarotti[1] · Mohamed Salahudeen[1] · Mario R. Romano[2] · Vito Romano[3,4] · Perumal Nithiarasu[5]

Received: 31 July 2017 / Accepted: 2 March 2018 / Published online: 22 March 2018

Abstract

The present work describes the application of the generalised porous medium model to study heat and fluid flow in healthy and glaucomatous eyes of different subject specimens, considering the presence of ocular cavities and porous tissues. The 2D computational model, implemented into the open-source software OpenFOAM, has been verified against benchmark data for mixed convection in domains partially filled with a porous medium. The verified model has been employed to simulate the thermo-fluid dynamic phenomena occurring in the anterior section of four patient-specific human eyes, considering the presence of anterior chamber (AC), trabecular meshwork (TM), Schlemm's canal (SC), and collector channels (CC). The computational domains of the eye are extracted from tomographic images. The dependence of TM porosity and permeability on intraocular pressure (IOP) has been analysed in detail, and the differences between healthy and glaucomatous eye conditions have been highlighted, proving that the different physiological conditions of patients have a significant influence on the thermo-fluid dynamic phenomena. The influence of different eye positions (supine and standing) on thermo-fluid dynamic variables has been also investigated: results are presented in terms of velocity, pressure, temperature, friction coefficient and local Nusselt number. The results clearly indicate that porosity and permeability of TM are two important parameters that affect eye pressure distribution.

Keywords Generalised porous medium model · Eye modelling · Aqueous humor flow · Intraocular pressure (IOP) · Patient oriented · Heat transfer

Nomenclature

C_f	Skin friction coefficient
c_p	Specific heat (J/g/K)
Da	Darcy number
F	Forchheimer coefficient
g	Gravity (m/s^2)
k	Thermal conductivity (W/m K)
L	Characteristic length (m)
n	Normal direction
Nu_L	Local Nusselt number
p	Pressure (Pa)
Pr	Prandtl number
t	Time (s)
T	Temperature (°C)
u	Velocity (m/s)

Greek symbols

α	Thermal diffusivity (m^2/s)
β	Thermal expansion coefficient (1/°C)
ε	Porosity
κ	Permeability (m^2)
μ	Viscosity (Pa s)
ρ	Density (kg/m^3)
τ_w	Wall shear stress (Pa)

✉ Alessandro Mauro
alessandro.mauro@uniparthenope.it

[1] Dipartimento di Ingegneria, Università degli Studi di Napoli "Parthenope", Centro Direzionale, Isola C4, 80143 Napoli, Italy

[2] Department of Biomedical Sciences, Humanitas University, Via A. Manzoni 113, 20089 Rozzano (Milan), Italy

[3] Department of Eye and Vision Science, Institute of Ageing and Chronic Disease, University of Liverpool, Liverpool, UK

[4] Moorfields Eye Hospital, London EC1V 2PD, UK

[5] Zienkiewicz Centre for Computational Engineering, College of Engineering, Swansea University, Swansea SA2 8PP, UK

Acronyms

AC	Anterior chamber
AH	Aqueous humor
CC	Collector channel
HE	Healthy eye
GE	Glaucomatous eye
IOP	Intraocular pressure
SC	Schlemm's canal
TM	Trabecular meshwork

Subscripts

e	Effective
f	Fluid
m	Mean
o	Ocular
ref	Reference
s	Solid

1 Introduction

Glaucoma is a group of eye diseases which may result in loss of vision due to damage of the optic nerve. In 2002, among the 37 million blind individuals worldwide, 12.3% were caused by glaucoma. By the year 2020, it is estimated that there will be about 80 million people in the world affected by glaucoma. Although different theories exist on its exact etiology, the underlying cause is still unclear [1]. The main risk factor for most types of glaucoma is the increased intraocular pressure (IOP), that is also the main focus of the curing treatments. IOP is a function of aqueous humor (AH) production by the ciliary processes of the eye, and its drainage through the trabecular meshwork. AH flows due to pressure differences between different areas, undergoing natural circulation, also induced by thermal gradients in ocular tissues. AH has a relevant role in maintaining physiological pressure conditions inside the ocular cavities, with serious implications on normal eye function. Apart from the function of balancing pressure at the anterior chamber (AC), AH aids in providing nutrients, removing waste, and transporting drug at the ocular tissues. Its motion is largely affected by the physical characteristics of the porous tissues, internal circulation due to mixed convection and outflow resistance at conventional pathways [2–4].

Numerous works have tried to elucidate the role of the porous characteristics of ocular tissues located in the vicinity of the iris-cornea on the fluctuations of IOP at the AC of an eye [5–16]. The majority of AH secreted by the ciliary body enters the AC and flows towards the conventional outflow pathway, encountering the trabecular meshwork (TM), Schlemm's canal (SC), collector channels (CC), and finally, episcleral venous system. The porous nature of the TM, investigated by many in vivo and in vitro studies, has been shown to affect AH flow resistance, with a significant effect on IOP [5–8]. Experimental studies have been carried out to find TM permeability of perfused human eye and have demonstrated the importance of this property on AH flow [9–13]. Moreover, the porosity of these tissues has been proved to influence AH outflow, due to the funnelling effect of small pores at the inner wall endothelium of SC that modulates the flow resistance at the TM [14–16].

Given the difficulties in experimentally analysing AH flow inside ocular cavities and tissues, different computational models have been developed for analysing the influence of AH outflow on IOP, often taking into account only the TM and not the whole anterior section of the eye [17–32]. Analytical and numerical models were developed to understand morphological changes at the TM due to IOP and its effects on TM permeability values based on Darcy's model [17–20]. These studies considered the 3D TM and obtained an analytical expression relating AH flow rate through the TM to pressure difference across it, due to TM permeability. Also, a 3D numerical study was carried out on the TM model with three different layers along with the inner wall endothelium of the SC [21]. This study demonstrated that there are disparities between heterogeneous and homogeneous permeability values of TM, with higher AH outflow resistance offered by the TM with heterogeneous permeability [21]. Moreover, several numerical heat transfer studies have been carried out to model laser therapy on the eyes and reported the temperature distributions in different regions of the eye including the AC in the absence of TM porous structure [22–24]. Eye models comprising both the AC and TM have also been developed, demonstrating that porous properties should be taken into account in eye modelling [25, 26]. These studies mainly focused on the therapeutic effects of drug delivery for glaucoma. In other numerical studies, models considering the TM structure were developed to analyse the effects of various parameters, like viscosity, permeability and flow rate on IOP, without considering the porosity effects on IOP in the presence of different configurations of the human eyes [27–29].

The literature survey clearly shows a strong interest of the biomedical engineering community in numerical modelling of the anterior section of the eye. Although significant efforts have been made, the effects of both porosity and permeability of TM on AH outflow and, consequently, on IOP, on subject-specific geometries are still lacking. These parameters play a crucial role on pressure management of an eye and thus must be properly analysed using the more available and suited comprehensive models, including non-Darcy models. Therefore, a general porous medium model that is able to take into account the effects of porosity and permeability and its interaction with porous tissues and free fluid can produce relevant information concerning AH outflow from the anterior chamber of an eye and its management of IOP.

In order to study the effects of TM porous structure on AH outflow and IOP, the authors propose here for the first time the use of the generalised porous medium (GPM) model that

integrates Darcy, Forcheimmer and Brinkmann models in the solution of fluid flow and heat transfer through porous media [33–40]. The present approach is particularly useful to reproduce the AH temperature and fluid flow distribution inside the anterior section of an eye, as it allows modelling fluid cavities, such as the AC, and porous tissues, TM, with one universal model. The 2D model has been implemented for the first time in the finite volume-based software, OpenFOAM (Open Field Operation And Manipulation), and it has been verified for a mixed convection benchmark problem of free fluid-porous medium interface. The model is then used for the first time within a patient-oriented procedure, to solve flow and heat transfer in four different subject-specific eyes, extracted from tomographic images of both healthy and glaucomatous patients. In particular, among these eyes, the doctors have diagnosed two glaucomatous patients with uveitic glaucoma, due to inflammation at TM cells, increase in AH outflow resistance and consequent increase of IOP at the AC [41]. Therefore, the authors have focused the present patient-oriented work on the study of the effects of TM flow resistance on AH thermo-fluid dynamics and increased IOP. The application of the present model allowed the authors to highlight the sensitivity of heat and mass transport phenomena occurring in human eyes to key eye parameters, such as porosity and permeability of ocular tissues and, consequently, understand the differences between healthy and glaucomatous eyes. From such parameters, flow, pressure and temperature fields within the anterior section of the four eyes have been reported. The IOP values measured on these patients have been used to calibrate the permeability and porosity values in the numerical simulation to be used in the generalised porous medium model. The authors aim at proving that these

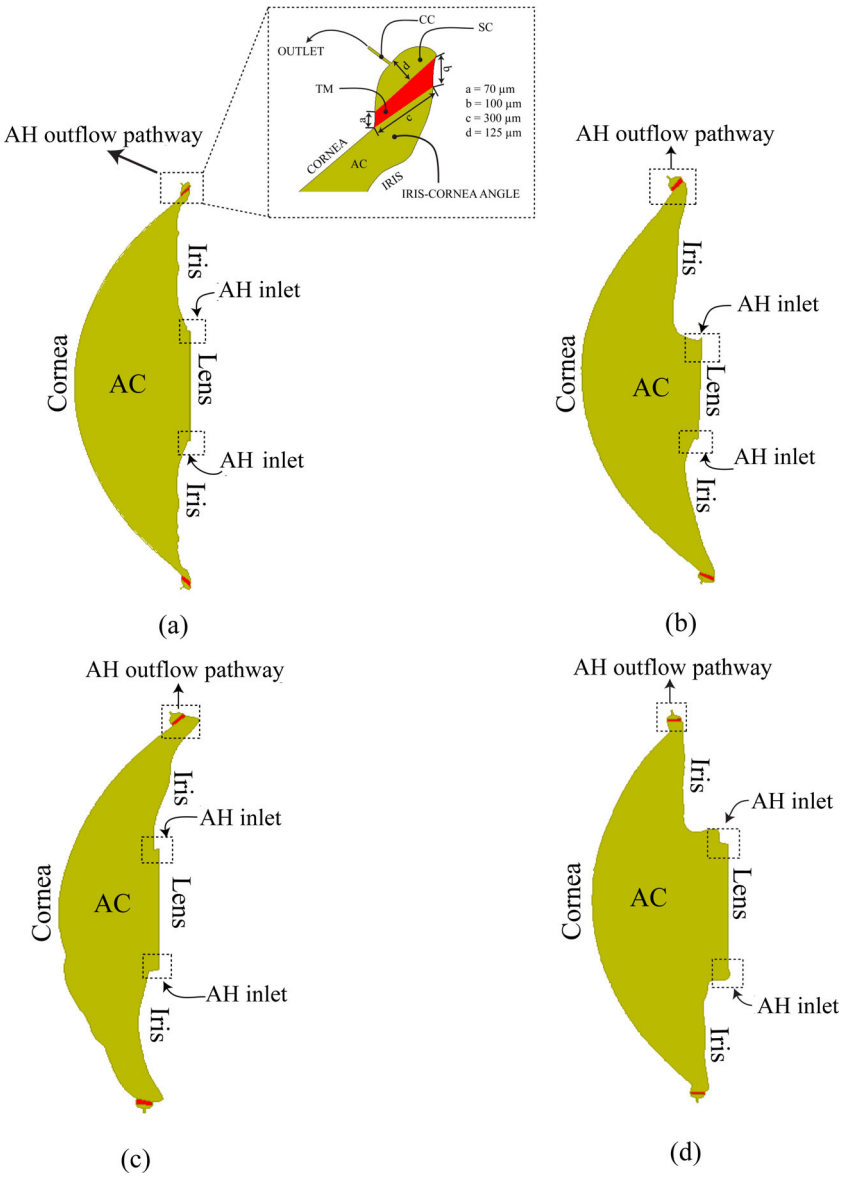

Fig. 1 Computational domains of the AC of human eyes: **a** HE1, **b** HE2, **c** GE1, **d** GE2

Table 1 Dimensions of the anterior segment of the eyes

No.	Tissue	Dimension (mm)		Source
		Present study (HE1)	Literature	
1	Cornea thickness	0.58	0.6	Narasimhan et al. [23], Ng and Ooi [44]
2	Anterior chamber length	10	11.8	Jooybar et al. [45]
3	Anterior chamber depth	3.2	3.8	Kapnisis et al. [28]
4	Iris thickness	0.45	0.35	Kapnisis et al. [28]
5	Pupil length	2.98	3.00	Kapnisis et al. [28]

properties drastically affect flow and thermal fields in the AC of the eyes and are strongly related to healthy and glaucomatous conditions.

The paper is organised as follows: the next section describes the mathematical model employed; the third section presents the numerical implementation within OpenFOAM; the fourth section reports the main numerical results obtained for the four eyes considered in this work and for the verification of the procedure. Some conclusions are drawn in the last section.

2 Mathematical model

The present study uses the GPM model to study AH flow and heat transfer inside the anterior segment of an eye and outflow through TM pathways. In order to simulate real-life problems, tomographic images of eyes from four different patients have been processed, and the computational domains have been extracted for numerical analysis, as shown in Fig. 1. Healthy conditions of these eyes, based on IOP, have been used to categorise the different patients; the first two eyes shown in Fig. 1a, b were healthy, while clinicians, who co-author this work, classified the third and fourth as glaucomatous eyes, namely GE1 (Fig. 1c) and GE2 (Fig. 1d). The measured IOP values of these four eyes were 14.1, 16, 18.9 and 27.0 mmHg, respectively. The computational domain size varies for the four eyes, especially the areas of the AC as shown in Fig. 1 that were measured to be respectively (a) 28.6 mm^2, (b)24.1 mm^2, (c) 25.2 mm^2 and (d) 33.2 mm^2 for the four patients.

The computational domain comprises the TM, SC and CC as shown in Fig. 1. The small segment between the lens and iris captured from the scans serves as the inlet for AH secreted by the ciliary body. CC, among the AH outflow pathway, are modelled as outlets for the AH. Table 1 reports the typical dimensions of the anterior segment of the eye as reported in the available literature and the values considered for the present simulations of the first healthy eye (HE1) of Fig. 1. The TM considered in the present model has widths of 70 and 100 μm at the anterior and posterior portion, respectively. Moreover, SC with a maximum height of 125 μm, based on the real anatomy of the structure, has been modelled at the top of the TM [12, 42, 43].

2.1 Governing equations

Laminar, incompressible fluid flow has been considered in this work for AH, in order to model its velocity and temperature inside the anterior chamber of human eyes by solving the GPM model [33–37]. Buoyancy effects have been incorporated via the Boussinesq approximation [46], relating density variations to temperature differences in the cornea, lens and iris, obtaining a mixed convection flow regime. The conservation equations of the generalised porous medium model in indicial notation can be written as:

Mass

$$\frac{\partial u_i}{\partial x_i} = 0 \tag{1}$$

Momentum

$$\frac{\rho_f}{\varepsilon}\left[\frac{\partial u_i}{\partial t} + \frac{\partial}{\partial x_j}\left(\frac{u_i u_j}{\varepsilon}\right)\right] = -\frac{1}{\varepsilon}\frac{\partial}{\partial x_i}(p_f \varepsilon) + \frac{\mu_e}{\varepsilon}\frac{\partial^2 u_i}{\partial x_i^2} - \frac{\mu_f u_i}{\kappa} - \frac{1.75}{\sqrt{150}}\frac{\rho_f}{\sqrt{\kappa}}\frac{|V|}{\varepsilon^{3/2}}u_i + (\rho_{ref} - \rho_f)g\gamma_i \tag{2}$$

Table 2 Thermal and physical properties of AH

No.	Parameter	Value	Unit
1	Density, ρ_f	998 [29]	kg/m^3
2	Viscosity, μ_f	7.5×10^{-4} [46]	kg/(m s)
3	Thermal expansion coefficient, β	3.0×10^{-4} [29]	1/K
4	Thermal conductivity, k	0.58 [52]	W/(m K)
5	Specific heat, c_p	4.2×10^3 [52]	J/(kg K)

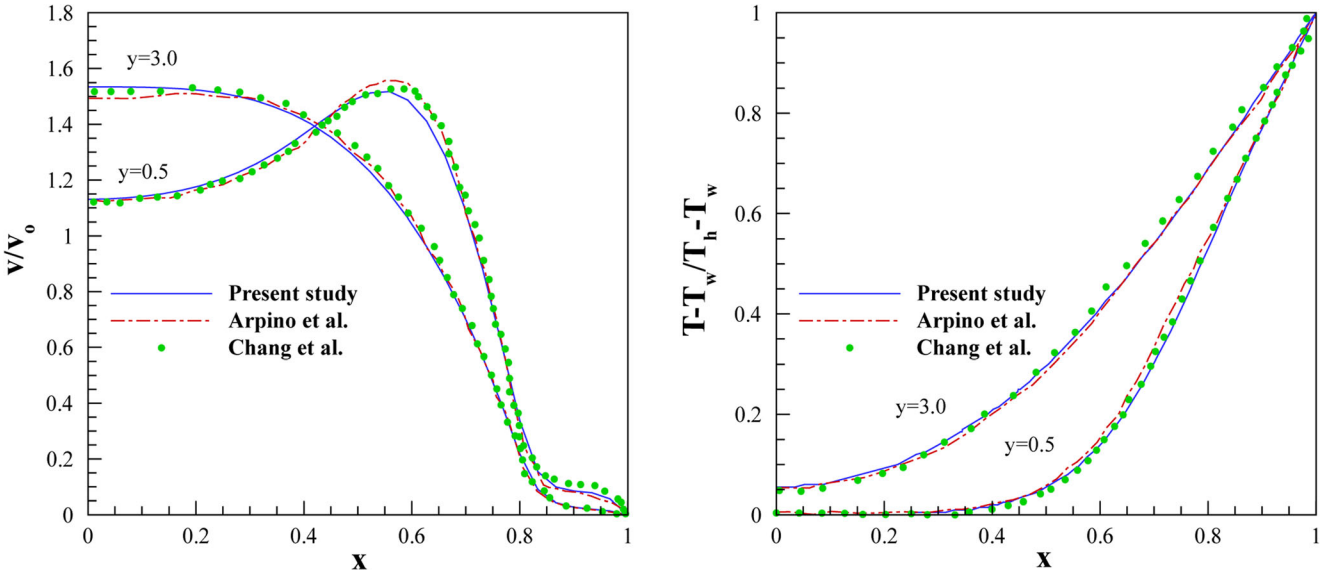

Fig. 2 Non-dimensionalised velocity (left) and temperature (right) profiles at $Da = 10^{-3}$

Boussinesq approximation is employed by treating $(\rho_{ref} - \rho_f)g = g\beta(T_{ref} - T)$, where T_{ref} is taken as the mean temperature between the iris and cornea.

Energy

$$\left[\varepsilon(\rho c_p)_f - (1-\varepsilon)(\rho c_p)_s\right]\frac{\partial T}{\partial t} + (\rho c_p)_f u_i \frac{\partial T}{\partial x_i} = k\left(\frac{\partial^2 T}{\partial x_i^2}\right) \quad (3)$$

The effective viscosity, μ_e, is assumed to be equal to AH viscosity. The generalised porous medium model (1–3) is very useful in problems where a porous medium interacts with a free fluid, such as the present case where ocular cavities are in contact with porous tissues. In fact, the model approaches the Navier-Stokes equations when permeability, κ, goes to infinity and porosity, ε, approaches unity. However, when permeability assumes a finite value and porosity is smaller than 1, the model describes heat and fluid flow in porous tissues. Therefore, the coupled problem can be easily solved with one set of equations (1–3) by using proper coefficients in the fluid and porous domains of the complex problem. According to Kozeny-Carman relation [47], porosity has a direct correlation with permeability, based on Darcy's law as given in Eq. (4):

$$\kappa = \frac{d_p^2 \varepsilon^3}{150(1-\varepsilon)^2} \quad (4)$$

where d_p is the average pore size.

2.2 Boundary conditions

AH is secreted by the ciliary body, which is represented in the present model by an inlet section in the anterior segment of the eye, between iris and lens, as shown in Fig. 1. A nominal volumetric flow rate of 2.5 μL/min is assigned at this inlet section [48, 49]. SC and CC are subject to an episcleral venous pressure of 10.5 mmHg [50, 51]. Lens, iris and cornea are assumed to be impermeable walls, where no slip boundary conditions are imposed. The temperature of the outer surface of cornea is set at 27 °C, while the temperature of lens and iris is set to normal human body temperature of 37 °C [46]. Appropriate permeability values, depending on the health condition of the human eye, are used for the porous tissue that

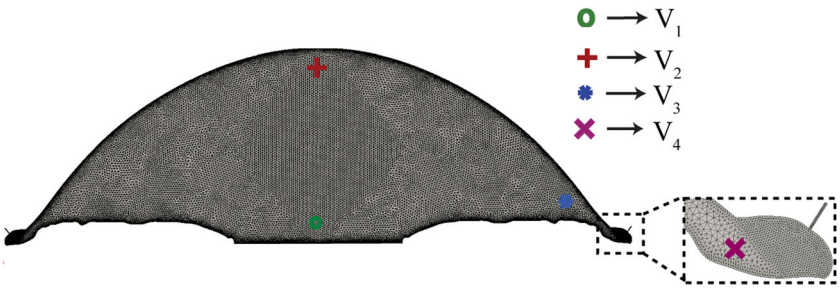

Fig. 3 Computational grid with 46,448 triangular elements

Table 3 Grid-independent study on C_f and Nu

No.	Elem. num.	C_f (cornea)	Difference (%)	C_f (iris)	Difference (%)	Nu (cornea)	Difference (%)	Nu (iris)	Difference (%)
1	65,842	0.390	–	0.540	–	6.510	–	10.442	–
2	46,448	0.388	0.50	0.538	0.37	6.489	0.32	10.439	0.02
3	41,640	0.387	0.76	0.537	0.55	6.475	0.54	10.433	0.09
4	38,138	0.386	1.02	0.536	0.74	6.460	0.76	10.431	0.10
5	31,212	0.381	2.37	0.520	3.70	6.445	0.99	10.420	0.20

represents the TM. The physical and thermal properties of AH are reported in Table 2.

3 Numerical implementation

OpenFOAM, a finite volume-based software written in C++ language, consists of a class of algorithms for solving different flow physics and heat transfer problems [53]. The solver implemented in the present work is customised to solve the generalised porous medium model for momentum and energy conservation equations (1–3). The equations have been modelled in the solver by adding the additional porous medium terms. The current study is focussed on steady state, and therefore, transient terms are not relevant to this work. The problem is solved by using a solver for steady, buoyant, incompressible flows, based on the pressure velocity coupled SIMPLE algorithm developed by Patankar and Spalding [54]. The under-relaxation parameters for velocity and pressure enhance the stability of the numerical procedure [54].

In order to fully exploit the flexibility of the generalised porous medium model in OpenFOAM, different domains were created for porous media and free fluid. In the geometry creation directory, *cellZones* have been created only for porous domains. The porous terms have been incorporated in a C++ file *createFile.H*, where the solver accesses these terms only while solving porous domains. The porosity assumes the value of 1 for the free fluid domains and its value in porous domain is taken from *transport properties* file. The sequence of operation for the above procedure can be described as follows:

- The momentum equation is discretised in space, and the set of linear equations solved implicitly to predict velocity. Since OpenFOAM employs a collocated grid arrangement, velocities are calculated and interpolated at the faces of the cell using the guessed pressure values and a source term [55].
- Energy equation is discretised and solved implicitly to calculate temperature. The effective kinematic density derived from Boussinesq approximation is updated based on the new temperature distribution.
- The pressure field is corrected at the cell centres with pressure Poisson equation.
- The resultant pressure field is employed to calculate the correct velocity. New sets of velocity and pressure values are then calculated by using the corrected velocity and pressure values.

4 Results

This section presents the results obtained by using the present numerical procedure. After verification of the code against a benchmark problem available for a mixed convection, flow and heat transfer in human eye models have been studied. In this work, the influence of the following parameters/quantities on the IOP has been considered: TM porosity and permeability, aqueous humor velocity, skin friction coefficient (C_f) and the local Nusselt number (Nu_L) at the surface of the cornea and iris. The porous structure of the TM has been analysed, as it directly influences the velocity field in the AC and, as a

Table 4 Grid-independent study on velocity

No.	Elem. num.	V_1 (mm/s)	Difference (%)	V_2 (mm/s)	Difference (%)	V_3 (mm/s)	Difference (%)	V_4 (mm/s)	Difference (%)
1	65,842	0.01528	–	0.05275	–	0.02327	–	0.05948	–
2	46,448	0.01527	0.072	0.05272	0.055	0.02319	0.335	0.05940	0.134
3	41,640	0.01512	1.020	0.05228	0.890	0.02296	1.323	0.05939	0.151
4	38,138	0.01511	1.130	0.05228	0.890	0.02273	2.315	0.05933	0.252
5	31,212	0.01495	2.140	0.05183	1.734	0.02262	2.805	0.05910	0.638

Table 5 Corneal temperature sensitivity analysis

No.	Corneal temperature (°C)	Maximum velocity at AC (mm/s)
1	27	1.20
2	30	0.70
3	32	0.50
4	35	0.15

consequence, the IOP. Moreover, the local Nusselt number (Nu_L) has also been analysed as it is an indication of heat transfer, that affects the AH flow and, therefore, IOP. The skin friction coefficient (C_f) indicates the shear stress due to the velocity gradient at ocular surfaces, calculated using AH velocity at the AC, and thus, indirectly influences pressure.

The authors have implemented the GPM model within a 2D approach, since the objective of the paper is to demonstrate the importance of taking into account the porous properties of ocular tissues for both healthy and glaucomatous eyes and highlight the differences between thermal and fluid dynamic quantities in healthy and glaucomatous eyes due to these properties, carrying out a comparative analysis. However, the authors have carried out a numerical analysis on a 3D eye model of HE1, finding out a maximum difference on the obtained velocity profiles at the horizontal section smaller than 5%. Therefore, given (i) the simplicity of the 2D model with respect to the 3D one, in particular concerning the reconstruction of the 3D domain and the computing time, and (ii) the difficulty in obtaining 3D eye images on the basis of traditional medical techniques, the 2D approach could be considered particularly suitable for the present comparative analysis. In the near future, the authors will extend the present 2D modelling approach, based on the GPM model, to 3D, focussing on patient-specific eyes. Future work will also take into account the integration of ocular drainage devices for glaucoma treatment [56] within the present model.

4.1 Verification: mixed convection in a partial porous vertical channel

This section reports a comparison between the numerical results obtained by using the present model and the data available in the literature for a 2D benchmark problem of mixed convection, i.e. vertical channel partially filled with a porous medium. All the details concerning the computational domain and boundary conditions can be found in references [36, 57]. Only half geometry is considered by taking advantage of the symmetry of flow and thermal fields. This is an example of fluid-saturated porous medium and free fluid interface problem in which the thickness of the free fluid layer is four times the thickness of the porous matrix. The right vertical wall is maintained at a higher temperature of $T_h = 37$ °C, while the fluid enters at the bottom of the domain with a prescribed velocity of $v_0 = 1$ m/s and a temperature of $T_w = 27$ °C.

The numerical results obtained with the OpenFOAM model developed in the present work are verified against the data available from the literature by Arpino et al. and Chang et al. [36, 57]. The parameters considered in the numerical analysis are $Da = 10^{-3}$, $Gr = 10^3$, $Re = 50$, $Pr = 0.72$ and $\varepsilon = 0.8$. It should be pointed out that this value of Darcy number is similar to the one encountered in eye models for the TM porous tissue, which is generally in the range of 10^{-4} to 10^{-3}.

The non-dimensional velocity and temperature profiles have been plotted along the flow direction, $y = 0.5$ and $y = 3$ in Fig. 2. It is clear from this figure that an excellent agreement

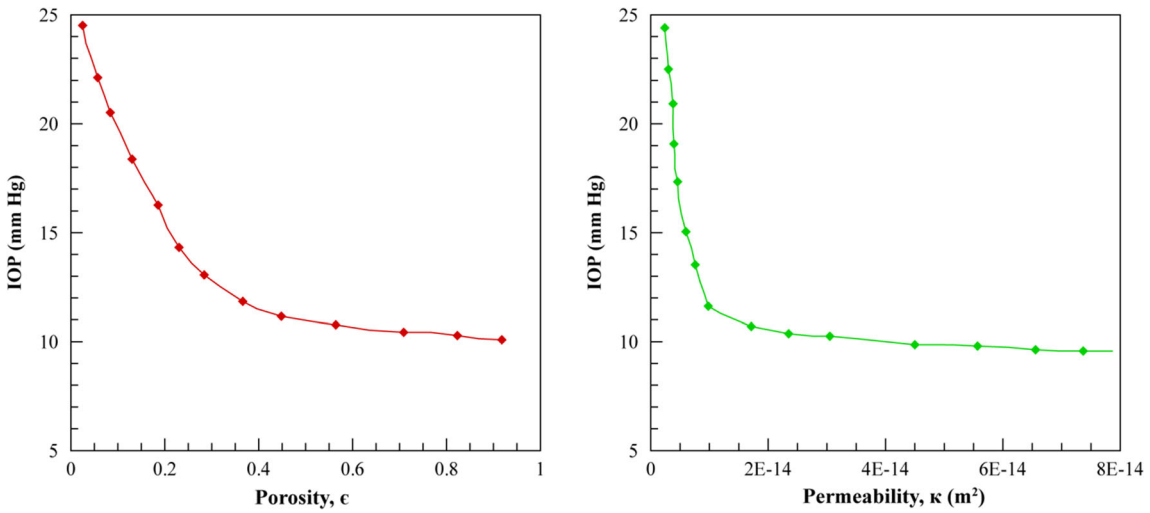

Fig. 4 IOP at AC with respect to TM porosity (left) and permeability (right)

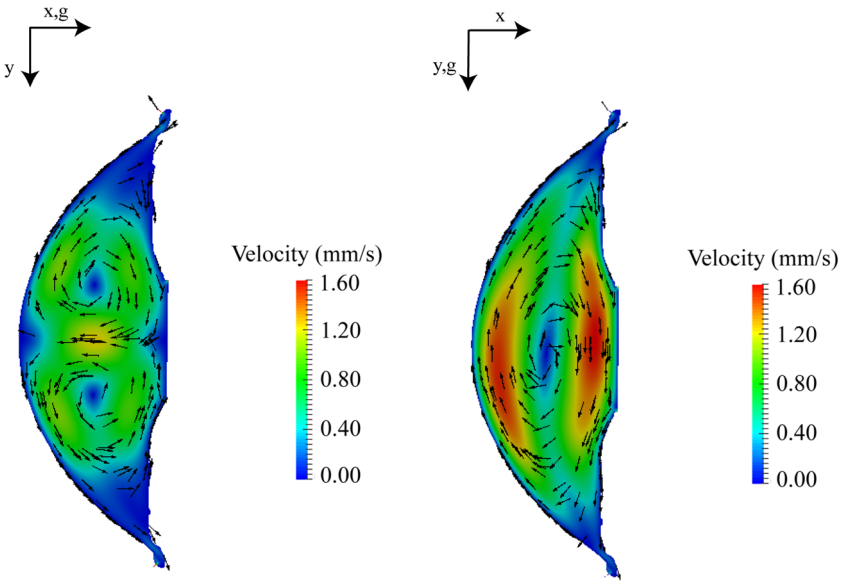

Fig. 5 Velocity contours and vectors for HE1 for supine (left) and standing (right) positions

with literature data has been obtained, both in terms of velocity and temperature. As seen, velocity values are much smaller in porous medium (for x between 0.8 and 1) than in the fluid layer. As expected, steep velocity gradients are observed at the interface between porous insert and free fluid.

4.2 Flow and thermal fields in different eye models

In this section, the results obtained for AH flow and heat transfer in four different eyes are reported. The current eye models can be considered as partial porous domains, since the TM is modelled as a porous matrix and the AC as a free fluid domain. A grid independence study has been carried out. The skin friction coefficient (C_f) and local Nusselt number (Nu_L) at the surface of the cornea and iris have been analysed.

4.2.1 Grid independence study

Figure 3 shows the computational grid of eye HE1, composed of 46,448 triangular elements. This mesh has been considered after a mesh sensitivity analysis, in order to ensure the best balance between computational time and accuracy. The average skin friction coefficient, C_f, and the average Nusselt number, Nu, along the cornea and iris surfaces have been

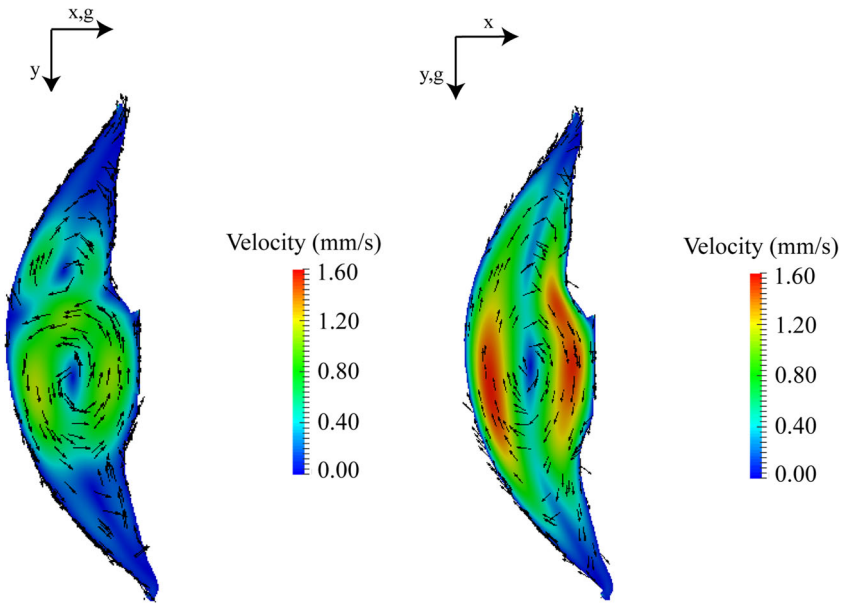

Fig. 6 Velocity contours and vectors for HE2 for supine (left) and standing (right) positions

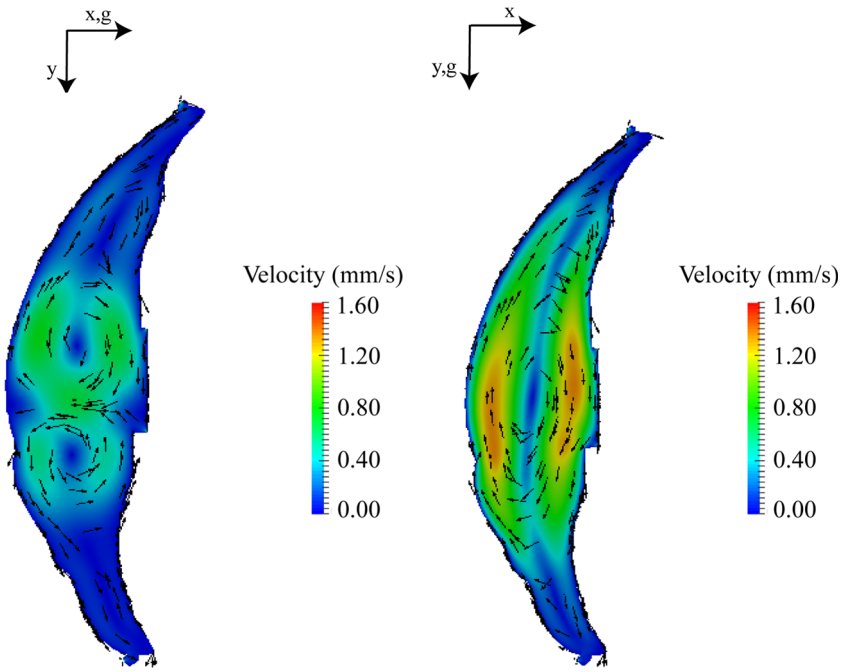

Fig. 7 Velocity contours and vectors for GE1 for supine (left) and standing (right) positions

calculated based on numerical results for five different grids, together with the velocity values at different points of the domain, reported in Fig. 3. These parameters, calculated for the finest grid, have been taken as reference, in order to calculate the percentage difference with the parameters obtained for the four grids. The results are reported in Tables 3 and 4. The grid with 46,448 triangular elements has been chosen for the simulations, since the percentage difference with respect to the finest grid is smaller than 1%. The same approach has been used for the other three eye geometries.

4.2.2 Sensitivity analysis on cornea temperature

A sensitivity analysis on different corneal temperatures for HE1 has been carried out. Table 5 shows the maximum velocity values calculated in the AC of HE1 in the supine condition for different temperature values of the corneal surface. As seen, the velocity magnitude inside AC increases when the corneal temperature decreases, due to the temperature difference between the surfaces of iris, lens and cornea.

Ng et al. [44] adopted an ambient temperature of 25 °C at the cornea for the analysis of temperature distribution in the

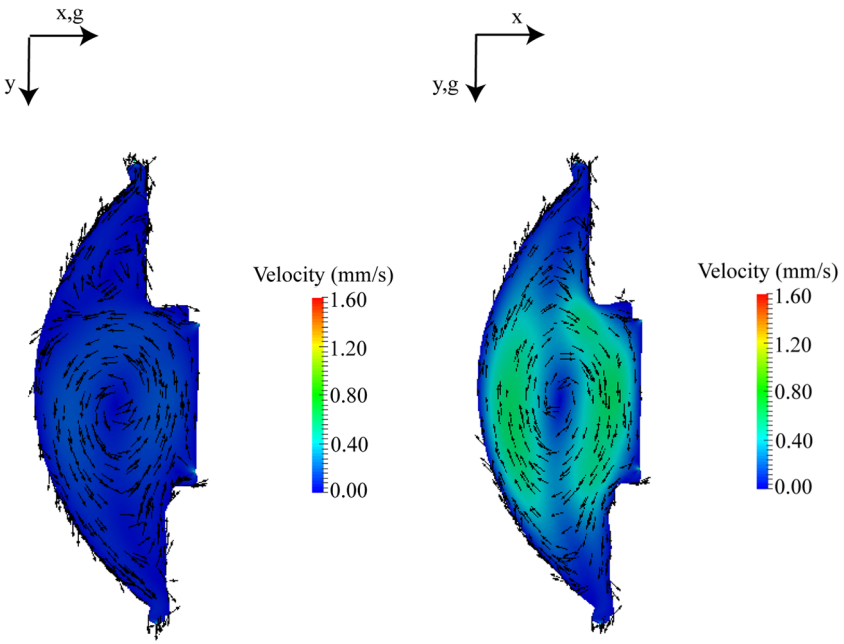

Fig. 8 Velocity contours and vectors for GE2 for supine (left) and standing (right) positions

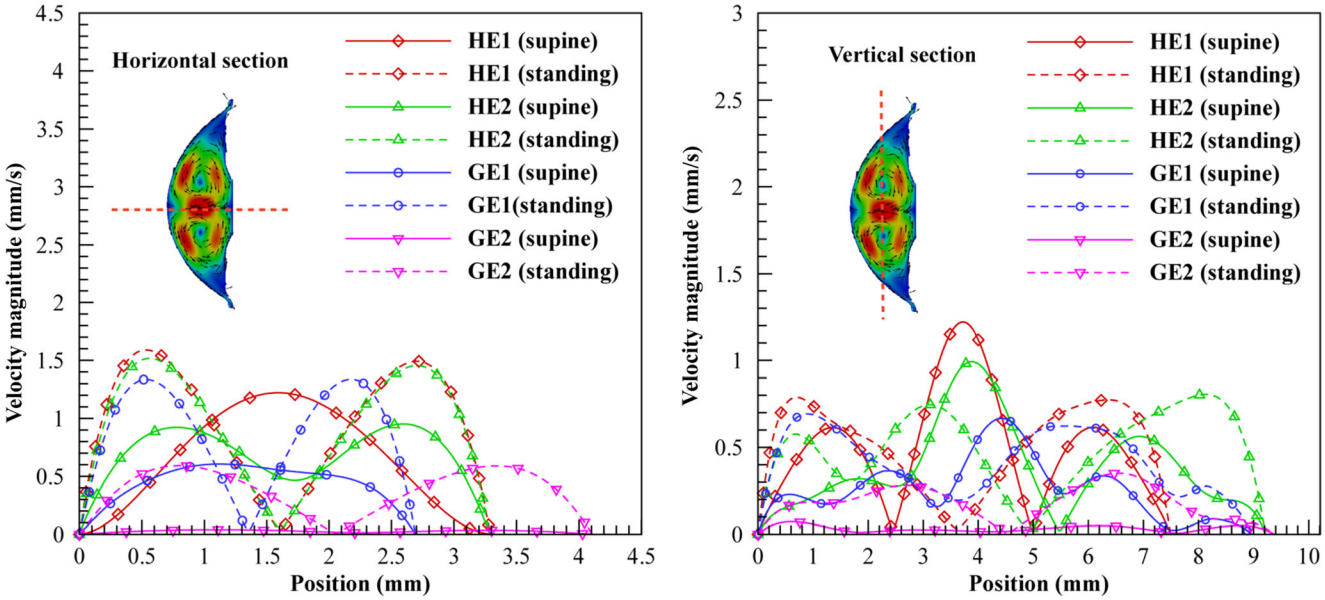

Fig. 9 Velocity profile along the horizontal (left) and vertical (right) sections of the eye for supine and standing positions for different eye models

AC, observing a maximum AH velocity of 0.0278 mm/s. The disparity between the results may be due to several reasons, such as the differences in the model, i.e. the absence of TM structure and the differences in computational domain and boundary conditions. In the numerical study of Villamarin et al. [29], a maximum AH velocity of 0.08 mm/s was reported at AC with a corneal surface temperature of 35 °C. Although these results are closer to the present results, the difference may be due to disparity in the computational domain, thermal boundary conditions and permeability values used between the studies. Given the substantial differences between the studies, it is important to include a model that is physically sensible and physiologically useful. Thus, it is important to take into account the presence of ocular porous tissues, with the corresponding physical properties, within the generalised porous medium model.

4.2.3 Effects of TM porosity and permeability on IOP

The primary resistance for the AH flow from the anterior chamber to the collector channels is due to the TM, and therefore, the influence of physical properties like permeability and porosity of TM on IOP is very important. The porous tissues in the TM have been considered in this present study to be isotropic and homogeneous.

Figure 4 shows the dependence of IOP on the porosity and permeability values implemented in the generalised porous medium model by means of numerical simulation. In the present study, the pathologies of the eyes GE1 and GE2 are due to uveitic glaucoma conditions that affect the physiology of trabecular meshwork pores and, consequently, increase the IOP at the AC.

According to medical considerations, IOP values above 21 mmHg usually correspond to glaucoma conditions, and IOP values above 18 mmHg can often be related to glaucoma risk conditions. These are general considerations, since this paper does not have the aim to investigate the different types of glaucoma, but aims at analysing the effects of TM porosity and permeability on IOP, by means of numerical modelling the AH thermo-fluid dynamics inside ocular cavities and porous tissues.

Therefore, in the present work, the authors have found, by means of numerical simulations, that glaucoma eyes should be characterised by TM permeability smaller than $4 \times 10^{-15} m^2$, that corresponds to porosity values smaller than 0.08. In this study, non-glaucoma control patients were considered having IOP values between 9 and 18–21 mmHg, with corresponding permeability values ranging between 8×10^{-14} and $5 \times 10^{-15} m^2$ with porosity values greater than 0.1. It is obvious from Fig. 4 that the correct range of IOP is reproduced with the values of porosity and permeability considered in this work. Based on the porosity and permeability range, the IOP values have been calibrated for the eye models considered in the current study, which are discussed in the next subsections.

4.2.4 Aqueous humor velocity

The AH produced at the ciliary body moves towards the anterior chamber of the eye and undergoes a circulation pattern due to density differences caused by the temperature gradient within the cornea, lens and iris. AH is produced mostly by active secretion by ciliary body, and the normal human volume flow rate is considered to be 2.4–3 μL/min [48, 49].

The position of the eye with respect to gravitational direction has a significant influence on the AH flow inside the AC.

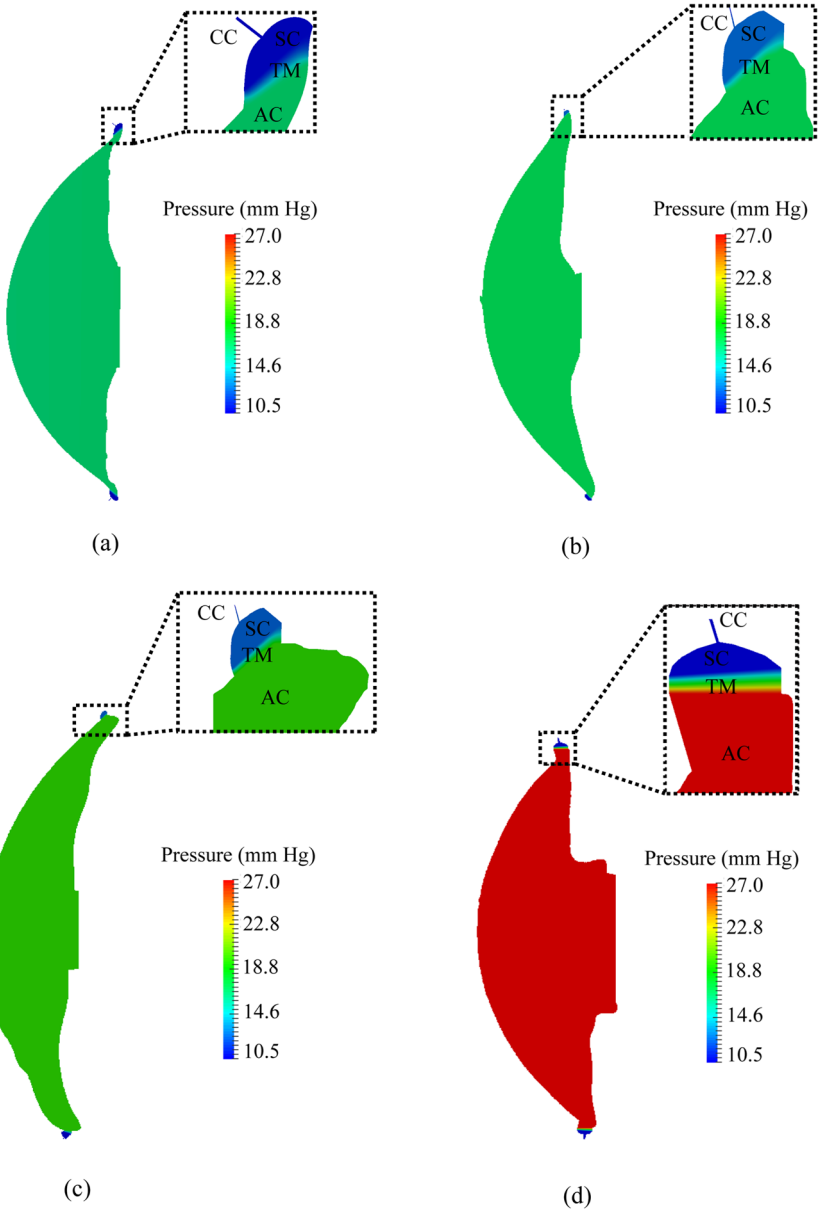

Fig. 10 Pressure contours for **a** HE1, **b** HE2, **c** GE1, **d** GE2

The present study considers both supine and standing positions, and Figs. 5, 6, 7 and 8 show the velocity vectors and velocity magnitude contours for supine and standing positions for the four different eyes considered. In the case of supine position, the AH flow forms two counter-rotating vortices at the core region of the AC. As seen, the AH coming from the ciliary body moves towards the mid-region of the AC and the corneal region, partly flowing towards the iris-cornea angle, while the remaining AH shifts towards the iris-lens direction to form vortices. In standing position, a single rotating vortex due to buoyancy effect is formed with AH velocity values larger than those calculated for supine position.

It can also be noticed that the flow in the first healthy eye HE1 has shown a more symmetric behaviour compared to HE2, GE1 and GE2 in supine conditions. The asymmetry in the patient-specific models of HE2, GE1 and GE2 invokes asymmetric AH circular patterns, particularly evident in supine position. It is interesting to note that, for supine position, there is a larger vortex located at the core region, characterised by higher velocity values with respect to the second smaller vortex. The magnitude of AH velocity is different in the four human eyes considered, and this variability is due to the different IOP and the values of TM porosity and permeability.

The velocity magnitude distributions across horizontal and vertical sections of each eye are plotted in Fig. 9. It can be noticed that for HE1 and HE2, the velocity profiles are symmetric for both supine and standing positions especially in the horizontal section, although they have a different pattern for supine position due to the different geometries of each eye. It is also interesting to note that the velocity values at both

horizontal and vertical sections of healthy eyes are larger than those corresponding to glaucoma eye models, for both supine and standing positions, due to TM permeability, with a consequent influence on IOP. The higher velocity observed in healthy eyes with respect to glaucoma eyes, GE1 and GE2, is due to the lower IOP, as described in the next subsection.

4.2.5 Intraocular pressure

Low permeability of TM produces high resistance to the AH flow, affecting IOP values. In practice, glaucoma is associated with structural changes in TM, characterised by a decrease in permeability and, consequently, an increase in IOP. The TM permeability values chosen for the four eyes have been correlated to approximately reproduce the IOP values in numerical simulation measured in clinical practice. Figure 10 shows the pressure contours calculated within the AC of all four eyes. The higher the resistance of the TM, the larger the pressure drop, and as a consequence, ophthalmologists focus their attention on the study of alternative pathways for the AH outflow from the AC. In the present study, an IOP of 14.1 mmHg is obtained for a TM permeability of $5.2 \times 10^{-15}\mathrm{m}^2$ in the HE1. The IOP values of 16, 18.9 and 27 mmHg are obtained for permeability values of 4.3×10^{-15}, 1.0×10^{-15} and $8.0 \times 10^{-16}\mathrm{m}^2$, respectively, in HE2, GE1 and GE2. The resistance to AH flow through the TM for the four eyes has been calculated as, respectively, 1.44, 2.20, 3.36 and 6.60 mmHg/μL/min.

4.2.6 Skin friction coefficient

As previously described, the velocity field in the AC varies depending on whether the patient is in supine or standing position. As noticed from the results, the flow is also heavily influenced by the values of porosity and permeability of the TM. This variability of velocity field has motivated the authors to analyse the shear stress at ocular surfaces, cornea and iris. The shear stress (τ_w) is calculated based on AH viscosity and velocity gradients on the ocular tissues as shown in Eq. (5). The skin friction coefficient (C_f) is expressed in terms of shear stress at the ocular surfaces (cornea, iris), density and mean velocity in the AC of the eye according to the following:

$$\tau_w = \mu \frac{\partial u}{\partial n} \tag{5}$$

$$C_f = \frac{\tau_w}{\frac{1}{2}\rho u_m^2} \tag{6}$$

where n is the normal direction to the ocular surface and u_m is the mean velocity magnitude in the AC.

The curve direction along which the C_f is calculated for the cornea and iris surfaces is shown in Fig. 11.

The skin friction coefficient, C_f, is plotted for supine and standing positions in Figs. 12 and 13 for the cornea and iris surfaces, respectively. The vortex patterns generated at the core region of the AC are due to buoyancy forces that induce higher velocity gradients at the cornea and iris surfaces.

Figure 12 shows the C_f distribution at the corneal surface for supine and standing positions. As seen, for HE1 (solid red line), C_f values are larger at the regions characterised by the thermally induced vortex and at the vicinity of the iris-cornea angle (refer to Figs. 5, 6, 7 and 8). Lower C_f values are observed at the mid-region of the corneal surface in supine position, where the AH is almost stagnant. Similar trends, with higher C_f values, are observed for HE1 at the iris surfaces (Fig. 13) in correspondence of the vortex regions and the iris-cornea angle. In the case of HE1 in standing position, C_f values at the

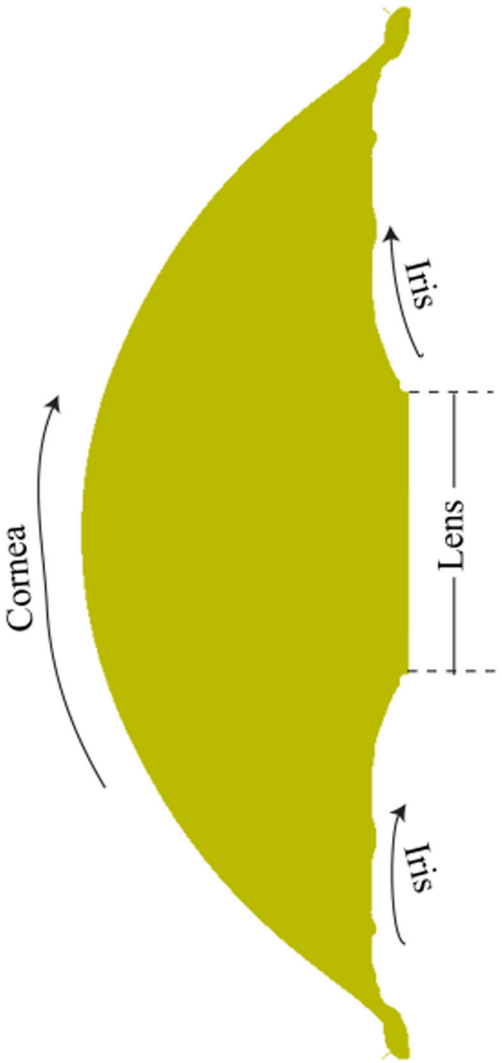

Fig. 11 Directions along which the skin friction coefficient is calculated for the cornea and iris

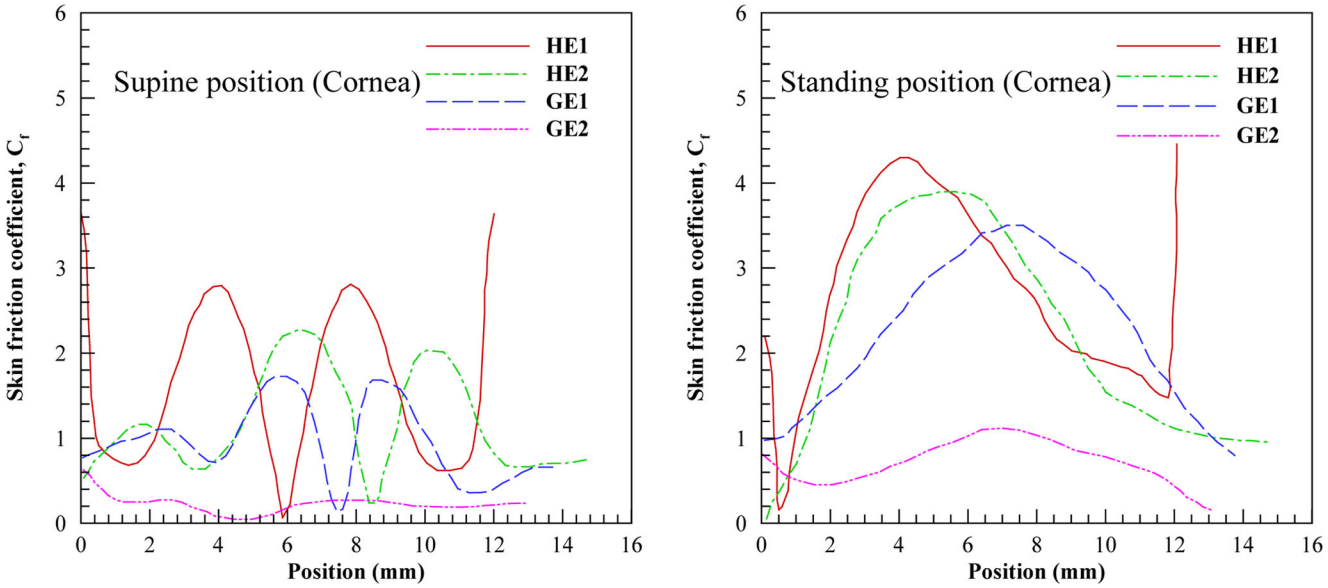

Fig. 12 Skin friction coefficient, C_f, profile along the cornea surface for supine (left) and standing (right) positions for different eye models

cornea and iris surfaces are higher than those considered for supine position, due to larger AH velocities at the core regions.

As noticed in Figs. 12 and 13, C_f values are slightly smaller for HE2 (dashed dot green line) and smaller for GE1 (dashed blue line) and GE2 (dashed dot dot pink line) with respect to HE1, due to the lower AH velocities. It is worthwhile to mention that glaucoma eyes appear to have the lowest C_f values among the eyes considered, suggesting a relation between this quantity and glaucomatous status of an eye.

4.2.7 Heat transfer

The local temperature differences within the cornea, iris and lens induce a density difference in the AH, invoking a hydrostatic pressure difference along the gravitational direction, creating vortices. Buoyancy forces play a major role in the enhancement of heat transfer due to the formation of vortices. AH at higher temperature flows from the iris and lens surfaces towards the lower temperature regions of the cornea, inducing temperature gradients at the core regions of the AC.

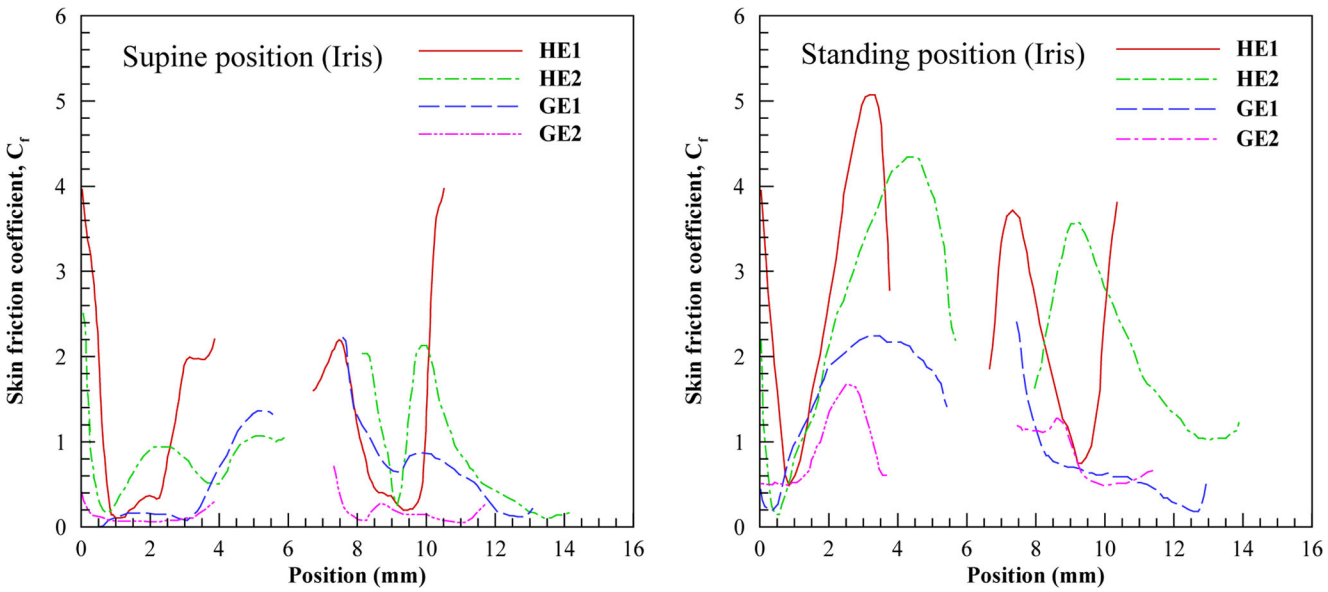

Fig. 13 Skin friction coefficient, C_f, profile along the iris surface for supine (left) and standing (right) positions for different eye models

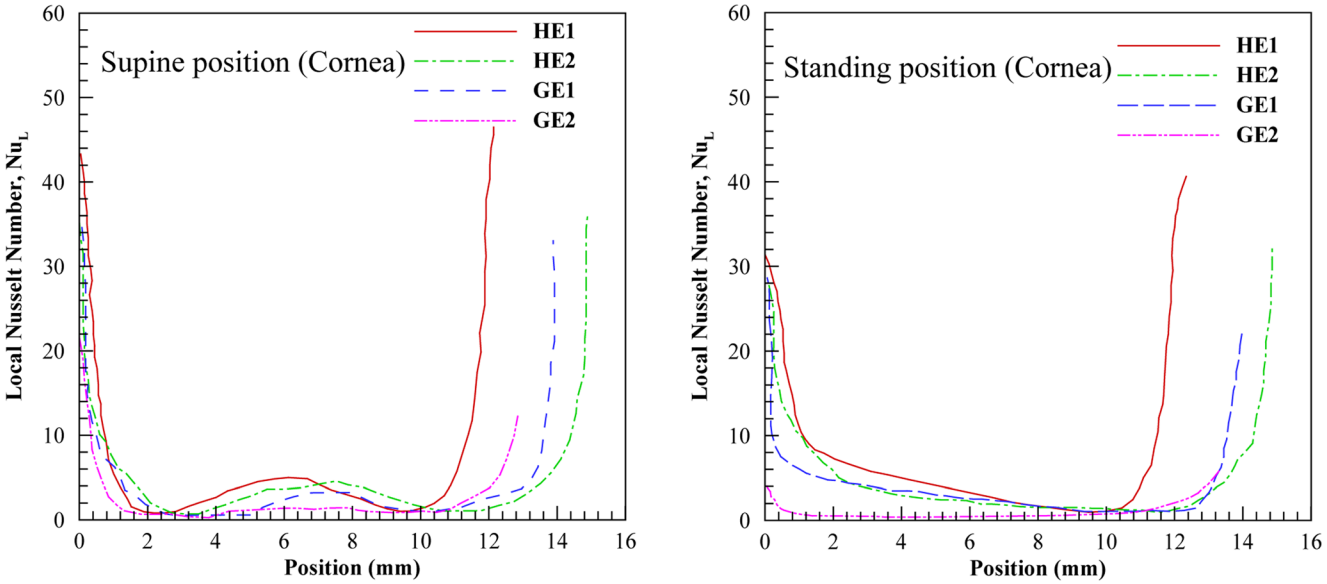

Fig. 14 Local Nusselt number, Nu_L, distribution along the cornea surface for supine (left) and standing (right) positions for different eye models

The heat transfer has been quantified and is calculated in terms of the local Nusselt number, Nu_L. Figures 14 and 15 present the Nu_L distribution for the cornea and iris along the same direction in which skin friction coefficient (C_f) is plotted. The local Nusselt number (Nu_L) has been calculated using the following equation:

$$Nu_L = \frac{\partial T}{\partial n} \times \frac{L}{T_0 - T_{ref}} \tag{7}$$

where L is the characteristic length, taken as AC width; n is the normal direction to the ocular surfaces (cornea, iris); and T_0 is the temperature at the cornea and iris.

The role of buoyancy forces in the enhancement of heat transfer is corroborated through higher values of Nu_L. In case of supine and standing positions of HE1 (Fig. 14), there is a gradual decrease in Nu_L from the iris-cornea angle to the regions of vortices (see Fig. 5). Beyond this point, an increase in heat transfer is observed. A higher heat transfer rate is observed at the corneal surface, located in the regions near the iris-cornea angle. Due to the close proximity of the cornea and iris surfaces, which causes an acceleration of the AH, an increase in Nu_L is observed. The Nu_L values for GE1 (dashed blue line) and GE2 (dashed dot dot pink line) at the corneal surface are smaller compared to those of HE1 (solid red line) and HE2 (dashed dot green line) due to the lower thermal convection. The higher velocity AH vortex patterns are more prominent at the iris surfaces for HE1 (Fig. 15) than for HE2, GE1 and GE2. As a consequence, a significant increase in Nu_L

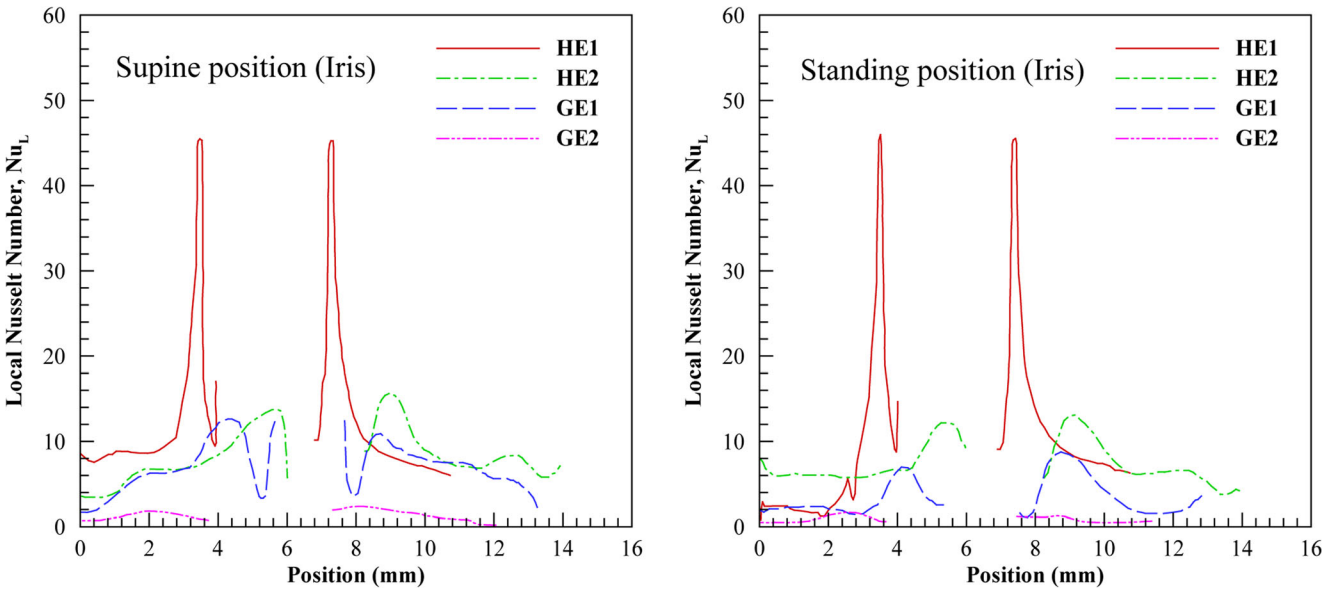

Fig. 15 Local Nusselt number, Nu_L, distribution along the iris surface for supine (left) and standing (right) positions for different eye models

is observed on the surface of the iris for HE1 (solid red line in Fig. 15) compared to HE2 (dashed dot green line), GE1 (dashed blue line) and GE2 (dashed dot dot pink line). As noticed, glaucomatous eyes show a clear distinction in heat transfer from HE1 and HE2 with lower Nu_L values.

5 Conclusions

In the present work, flow and heat transfer in four subject-specific human eyes have been studied by implementing the Generalized Porous Medium (GPM) model, coupled to patient-specific scans and measurements. The objective of the paper is to demonstrate the importance of taking into account the porous properties of ocular tissues for both healthy and glaucomatous eyes and highlight the differences between thermal and fluid dynamic quantities in healthy and glaucomatous eyes due to these properties, carrying out a comparative analysis.

The present results have been obtained with a 2D approach, given the simplicity of 2D models, directly constructed from actual 2D scans, with respect to 3D ones, in terms of reconstruction of the domain and computing time. For this reason, the 2D approach has been considered particularly suitable for the present comparative analysis.

The authors have analysed two healthy eyes and two glaucomatous eyes, in order to investigate the relevant role of porosity and permeability of the Trabecular Meshwork (TM), the primary site of Aqueous Humor (AH) flow resistance, on Intraocular Pressure (IOP) for different human physiological conditions.

Since the TM tissues are porous in nature, porous properties of TM have been taken into account here for the first time by using the GPM model, implemented within the open-source software OpenFOAM. The porosity and permeability values, to be used in the simulations, are calibrated based on the IOP values measured in a clinical trial for the four human eyes under investigation. Both flow and heat transfer results clearly indicate that the quantities of interest calculated in this work are substantially different for the glaucomatous eyes when compared to the healthy eyes. Due to lower values of TM porosity and permeability in the glaucomatous eyes, higher flow resistance and, thus, higher IOP are observed.

Subject specificity in the modelling of flow and heat transfer in human eyes should be considered, since the physiological conditions of the eyes vary from patient to patient. In particular, the glaucomatous eyes (GE1 and GE2) exhibit a lower AH velocity magnitude with respect to healthy eyes, due to higher IOP, affecting the normal biological function of the eye. Furthermore, the near wall quantities, i.e. skin friction coefficient (C_f) and local Nusselt number (Nu_L) at the cornea and iris, are influenced by the change in the health condition of the eyes. In the glaucoma eye models (GE1 and GE2), these quantities are lower than in the healthy eye models (HE1, HE2). The geometric difference of the eye models affects the AH dynamics inside the AC, due to the formation of distinctive vortex patterns (in supine position). Furthermore, the variations in thermo-fluid dynamic parameters for different eye conditions are noticeable and should be included in the understanding and treatment of eye disorders, using curing techniques like drug delivery and surgical methods.

The results obtained in this work prove the importance of using the generalised porous medium model, coupled to a patient-specific approach, to study the role of porous properties of ocular tissues in determining glaucomatous and healthy conditions for human eyes.

Funding information Alessandro Mauro, Nicola Massarotti and Mario R. Romano gratefully acknowledge the financial support of TeVR SIR project no. RBSI149484, CUP E62I15000760008. Alessandro Mauro also gratefully acknowledges the local program of the University of Napoli "Parthenope" for the support to individual research.

Compliance with ethical standards

The study was conducted according to the tenets of the Declaration of Helsinki.

References

1. Quigley HA, Broman AT (2006) The number of people with glaucoma worldwide in 2010 and 2020. Br J Ophthalmol 90:262–267
2. Johnson M, Mclaren JW, Overby DR (2017) Unconventional aqueous humor outflow: a review. Exp Eye Res 158:94–111
3. Bill A, Phillips CI (1971) Uveoscleral drainage of aqueous humor in human eyes. Exp Eye Res 12:275–281
4. Fan BJ, Wiggs JL (2010) Glaucoma: genes, phenotypes, and new directions for therapy. J Clin Investig 120:3064–3072
5. Braunger BM, Fuchshofer R, Tamm ER (2015) The aqueous humor outflow pathways in glaucoma: a unifying concept of disease mechanisms and causative treatment. Eur J Pharm Biopharm 95:173–181
6. Dautriche CN, Xie Y, Sharfstein ST (2014) Walking through trabecular meshwork biology: towards engineering design of outflow physiology. Biotechnol Adv 32:971–983
7. Stamer WD, Braakman ST, Zhou EH, Ethier CR, Fredberg JJ, Overby DR, Johnson M (2015) Biomechanics of Schlemm's canal endothelium and intraocular pressure reduction. Prog Retin Eye Res 44:86–98
8. Acott TS, Kelley MJ (2008) Extracellular matrix in the trabecular meshwork. Exp Eye Res 86:543–561
9. Allingham RR, Dekater AW, Ethier CR, Anderson PJ, Hertzmark E, Epstein DL (1992) The relationship between pore density and outflow facility in human eyes. Investig Ophthalmol Vis Sci 33:1661–1669
10. Grant WM (1958) Further studies on facility of flow through trabecular meshwork. A.M.A Archives of Ophthalmology. https://doi.org/10.1001/archopt.1958.00940080541001
11. Moses RA (1979) Circumferential flow in Schlemm's canal. Am J Ophthalmol 88:585–591
12. Johnson MC, Kamm RD (1983) The role of Schlemm's canal in aqueous outflow from the human eye. Investig Ophthalmol Vis Sci 24:320–325

13. Lutjen-Drecoll E (1973) Structural factors influencing outflow facility and its changeability under drugs. Investig Ophthalmol 12:280–294
14. Pedrigi RM, Stamer D, Reed A, Overby DR (2011) A model of giant vacuole dynamics in human Schlemm's canal endothelial cells. Exp Eye Res 92:57–66
15. Scott PA, Overby DR, Freddo TF, Gong H (2007) Comparative studies between species that do and do not exhibit the washout effect. Exp Eye Res 84:435–443
16. Braakman ST, Pedrigi R, Read AT, Smith JA, Stamer WD, Ethier CR, Overby DR (2014) Biomechanical strain as a trigger for pore formation in Schlemm's canal endothelial cells. Exp Eye Res 127:224–235
17. Ayyalasomayajula A, Park RI, Simon BR, Geest JPV (2016) A porohyperelastic finite element model of the eye: the influence of stiffness and permeability on intraocular pressure and optic nerve biomechanics. Comput Meth Biomech Biomed Eng 19:591–602
18. Eklund A, Linden C, Backlund T, Andersson BM, Lindahl OA (2003) Evaluation of applanation resonator sensors for intraocular pressure measurement: results from clinical and in vitro studies. Med Biol Eng Comput 41:190–197
19. Avtar R, Srivastava R (2007) Modelling aqueous humor outflow through trabecular meshwork. Appl Math Comput 189:734–745
20. Avtar R, Srivastava R (2006) Aqueous outflow in Schlemm's canal. Appl Math Comput 174:316–328. https://doi.org/10.1016/S0096300305004583
21. Bradley M, Heys JJ (2008) Effect of variable permeability on aqueous humor flow. Appl Math Comput 196:371–380
22. Wessapan T, Rattanadecho P (2014) Influence of ambient temperature on heat transfer in the human eye during exposure to electromagnetic fields at 900 MHz. Int J Heat Mass Transf 70:378–388
23. Narasimhan A, Kumar JA, Gopal L (2010) Transient simulations of heat transfer in human eye undergoing laser surgery. Int J Heat Mass Transf 53:482–490
24. Amara EH (1995) Numerical investigations on thermal effects of laser-ocular media interaction. Int J Heat Mass Transf 38:2479–2488
25. Ferreira JA, Oliveira PD, Pascoal S, Joaquim M (2014) Numerical simulations of aqueous humor flow: from healthy to pathologic situations. Appl Math Comput 226:777–792
26. Chen H, Zhang F, Huang Y, Jiankang W (2015) Numerical investigation of topical drug transport in anterior human eye. Int J Heat Mass Transf 85:356–366
27. Crowder TR, Ervin VJ (2013) Numerical simulations of fluid pressure in the human eye. Appl Math Comput 219:11119–11133
28. Kapnisis K, Doormaal MV, Ethier CR (2009) Modeling aqueous humor collection from human eye. J Biomech 42:2454–2457
29. Villamarin A, Roy S, Hasballa R, Vardoulis O, Reymond P, Stergiopulos N (2012) 3D simulation of the aqueous flow in the human eye. Med Eng Phys 34:1462–1470
30. Xiong G, Zhan J, Zuo K, Li J, Rong L, Xu G (2008) Numerical flow simulation in the post-endoscopic sinus surgery nasal cavity. Med Biol Eng Comput 46:1161–1167
31. Perez JF, Barea R, Boquete L, Hidalgo MA, Dapena M, Vilar G, Dapena I (2008) Cataract surgery simulator for medical education & finite element/3D human eye model. IFMBE Proc 20:429–432
32. Deplano V, Bertolotti C, Boiron O (2001) Numerical simulations of unsteady flows in a stenosed coronary bypass graft. Med Biol Eng Comput 39:488–499
33. Massarotti N, Nithiarasu P, Zienkiewicz OC (2001) Natural convection in porous medium-fluid interface problems: a finite element analysis by using the CBS procedure. Int J Numer Methods Heat Fluid Flow 11(5):473–490
34. Arpino F, Massarotti N, Mauro A (2011) Efficient three-dimensional FEM based algorithm for the solution of convection in partly porous domains. Int J Heat Mass Transf 54:4495–4506
35. Massarotti N, Ciccolella M, Cortellessa G, Mauro A (2016) New benchmark solutions for transient natural convection in partially porous annuli. Int J Numer Methods Heat Fluid Flow 26:1187–1225
36. Arpino F, Cortellessa G, Mauro A (2015) Transient thermal analysis of natural convection in porous and partially porous cavities. Numerical Heat Transfer Part A: Appl 67:605–631
37. Arpino F, Massarotti N, Mauro A (2010) A stable explicit fractional step procedure for the solution of heat and fluid flow through interfaces between saturated porous media and free fluids in presence of high source terms. Int J Numer Methods Eng 83:671–692
38. Alazmi B, Vafai K (2001) Analysis of fluid flow and heat transfer interfacial conditions between porous medium and a fluid layer. Int J Heat Mass Transf 44:735–1749
39. Vafai K, Kim SJ (1990) Fluid mechanics of the interface region between a porous medium and a fluid layer—an exact solution. Int J Heat Fluid Flow 11:1254–1256
40. Vafai K, Kim SJ (1990) Analysis of surface enhancement by a porous substrate. J Heat Transf 112:700–706
41. Siddique SS, Suelves AM, Baheti U, Foster CS (2013) Glaucoma and uveitis. Survey Opthalmol 58:1–10
42. Tandon PN, Autar R (1991) Biphasic model of the trabecular meshwork in the eye. Med Biol Eng Comput 29:281–290
43. Irshad FA, Mayfield MS, Zurakowski D, Ayyala RS (2010) Variation in Schlemm's canal diameter and location by ultrasound biomicroscopy. Ophthalmology 117:916–920
44. Ng EY, Ooi EH (2007) Ocular surface temperature: a 3D FEM prediction using bioheat equation. Comput Biol Med 37:829–835. https://doi.org/10.1016/j.compbiomed.2006.08.023
45. Jooybar E, Abdekhodaie MJ, Farhadi F, Cheng Y (2014) Computational modeling of drug distribution in the posterior segment of the eye: effects of device variables and positions. Math Biosci 255:11–20
46. Heys JJ, Barocas VH (2002) A Boussinesq model of natural convection in the human eye and the formation of Krukenberg's spindle. Ann Biomed Eng 30:392–401
47. Siggers JH, Ethier CR (2012) Fluid mechanics of the eye. Annu Rev Fluid Mech 44:347–372
48. Maus TL, Brubaker RF (1999) Measurement of aqueous flow by fluorophotometry in the presence of a dilated pupil. Investig Ophthalmol Vis Sci 40:542–546
49. McLaren JW (2009) Measurement of aqueous humor flow. Exp Eye Res 88:641–647
50. Mäepea O, Bill A (1989) The pressures in the episcleral veins, Schlemm's canal and the trabecular meshwork in monkeys: effects of changes in intraocular pressure. Exp Eye Res 49:645–653
51. Sit AJ, Ekdawi NS, Malihi M, McLaren JW (2011) A novel method for computerized measurement of episcleral venous pressure in human. Exp Eye Res 92:537–544
52. Emery AF, Kramar P, Guy AW, Lin JC (1975) Microwave induced temperature rises in rabbit eyes in cataract research. J Heat Transf 97:123–128
53. Weller HG, Tabor G, Jasak H, Fureby C (1998) A tensorial approach to computational continuum mechanics using object-oriented techniques. Comput Phys 12:620. https://doi.org/10.1063/1.168744
54. Patankar SV, Spalding DB (1972) A calculation procedure for heat, mass and momentum transfer in three-dimensional parabolic flows. Int J Heat Mass Transf 15:1787–1806. https://doi.org/10.1016/0017-9310(72)90054-3
55. Passalacqua A, Fox RO (2011) Implementation of an iterative solution procedure for multi-fluid gas-particle flow models on unstructured grids. Powder Technol 213:174–187
56 Mauro A, Romano MR, Romano V, Nithiarasu P (2018) Suprachoroidal shunts for treatment of glaucoma. Int J Numer Methods Heat Fluid Flow 28(2):297–314
57. Chang WJ, Chang WL (1996) Mixed convection in vertical parallel plate channel partially filled with porous media of high permeability. Int J Heat Mass Transf 39(7):1331–1342

Prof. Alessandro Mauro is Professor of Applied Thermodynamics and Thermal Science and coordinator of the medical-engineering group. His Ph.D. thesis was awarded with the Emerald Engineering Outstanding Doctoral Research Award in the category Numerical Heat Transfer & CFD. He is the author of more than 60 papers in this field.

Prof. Nicola Massarotti is Full Professor of Fluid and Thermal Sciences. He got his Ph.D. at the University of Wales Swansea. He is the author of more than 140 papers in the field of thermo-fluid dynamics and the head of LATEC lab in the University of Naples "Parthenope".

Mr. Mohamed Salahudeen is a Ph.D. student in the Department of Engineering at the University of Naples "Parthenope". He got the M.Sc. at IIT Madras, India. His research interests concern the application of thermo-fluid dynamic models to human eyes. He has 2 journal publications and 5 conference papers.

Prof. Mario R. Romano is an ophthalmologist and surgeon and Associate Professor at Humanitas University. He is recognised at the international level as an expert in ocular pathologies and is the author of more than 140 papers in this field.

Dr. Vito Romano is an ophthalmologist and surgeon and a research fellow at the University of Liverpool and Corneal fellow at Moorfields Eye Hospital. He is an expert in glaucoma therapies and the author of more than 100 papers in this field.

Prof. Perumal Nithiarasu is recognised at the international level as an expert of numerical modelling, porous media and biomedical applications. He is the author of more than 140 papers in these fields and received more than 2400 citations.